Effects of advanced laser processing on the microstructure and residual stresses of H13 tool steel

Trojan, Karel; Ocelík, Václav; Ganev, Nikolaj; Němeček, Stanislav; Čapek, Jiří

Published in:
EAN 2017 - 55th Conference on Experimental Stress Analysis 2017

EAN 2017
55th conference on experimental stress analysis

Effects of Advanced Laser Processing on the Microstructure and Residual Stresses of H13 Tool Steel

Karel Trojan[1,a], Václav Ocelík[2,b] , Nikolaj Ganev[1,c], Stanislav Němeček[3,d] and Jiří Čapek[1,e]

[1]CTU in Prague, Department of Solid State Engineering, Faculty of Nuclear Sciences and Physical Engineering, Trojanova 13, 120 00 Prague 2, Czech Republic

[2]Department of Applied Physics, Zernike Institute for Advanced Materials, Materials Science group, University of Groningen, Nijenborgh 4, 9747 AG, Groningen, The Netherlands

[3]RAPTECH s.r.o.,U Vodárny 473, 330 08 Zruč-Senec, Czech Republic

[a]karel.trojan@fjfi.cvut.cz, [b]v.ocelik@rug.nl, [c]nikolaj.ganev@fjfi.cvut.cz, [d]nemecek@raptech.cz [e]jiri.capek@fjfi.cvut.cz

Keywords: laser processing; cladding; residual stresses; microstructure; H13 tool steel.

Introduction

High power lasers are nowadays the standard in many different industrial fields which require precision, accuracy and high production efficiency. Therefore the paper outlines the capability of the advanced laser processing for additive manufacturing in relation to [1]. Hot working tool steel H13 is one of the most common die material used in metal and casting industries. Dies suffer great wear and thermo-dynamic stresses during their lifetime [1]. Therefore, various methods have been developed of repair. A great benefit of laser cladding in this field is a high productivity along with minimal influence on surrounding material by thermal stress [2]. This study reports an investigation of residual stresses (RS) obtained by X-ray diffraction (XRD) and microstructure (chemical and phase composition, crystallite orientation) obtained by orientation imaging microscopy (OIM) using electron backscattering diffraction (EBSD) and energy-dispersive X-ray spectroscopy (EDS) with scanning electron microscopy (SEM) of laser cladded tool steel AISI H13 on the classical construct steel S355 substrate. The research aimed to describe the residual stresses and microstructural parameters that are one of the most important factors that influence the products behaviour, especially fatigue life [3].

Experimental

Laser cladding was carried using a diode laser *Laserline* 5,5kW with optical head *Precitec Y52*. Laser power density 108 J/mm^2 was applied to form a single clad with the length 137 mm, width 6 mm and height approx. 1 mm above substrate. Powder of the tool steel AISI H13 was used with average particles diameter 53.1 ± 15.9 μm.

For X-ray diffraction analysis, the diffractometer *X'Pert PRO MPD* with Cr tube anode was used with pinholes, determining irradiated area of primary beam, size of 1×0.5 mm^2 in direction L and 2×0.25 mm^2 in direction T. Diffraction angles $2\theta^{211}$ were determined from the peaks of the diffraction lines $K\alpha_1\alpha_2$ of planes {*211*} of α-Fe which were fitted by *Centre of Gravity* function. For residual stress determination, $\sin^2\psi$ method and X-ray elastic constants $½s_2$ = 5.76 TPa^{-1} and s_1 = –1.25 TPa^{-1} were used.

In order to determine the phase composition of the surface layer, diffraction patterns were obtained by measuring clad on the instrument *X'Pert PRO MPD* in classical Bragg – Brentano (BB) focusing configuration with Co tube anode and 1×0.25 mm^2 pinholes. Measured diffractograms were processed with the program *X'Pert HighScorePlus* and crystalline phases were identified using a database *PDF-2*. Quantitative analysis was evaluated using the Rietveld analysis in the software *TOPAS 4.2*. The effective depth of penetration is corresponding to the thickness of the surface layer that provides about 63% of the diffracted intensity. By using these wavelengths, an effective penetration depth is about 5 μm.

The OIM data was collected using a Philips XL 30 FEG scanning electron microscope equipped with a *TSL OIM system* based on *DigiView 3* camera and *EDS EDAX SUTW+* detector. The accelerating voltage of 25 kV and 0.4 μm step size of scanning was used. A grain boundary is defined in the microstructure as a boundary between two neighbouring scanning points having crystallographic misorientation lager than 5°. All EBSD data were analysed with *TSL OIM Analysis 7.3.0* software and *Confident index* higher than 0.05. *Confident index* is based on voting scheme during automated indexing of the diffraction pattern where it is counted as a ratio of votes for the best solution minus votes for the second best solution divided by total possible number of votes from the detected Kikuchi bands. Certain crystallographic orientation receives a vote when observed angles between the three bands are same as table values of given orientation. Confident index 0.05 corresponds on an fcc material to approx. 70% probability of correct indexing.

Results and discussion

Table 1 gives the range of the chemical composition determined by ISO 4957 [4], the next row shows average chemical composition and standard deviation obtained by EDS on a cross-section of four randomly selected particles of the powder and the last line shows the average chemical composition and standard deviation in four different areas with dimensions approx. 500×250 μm^2. SEM image of the cross-section of the single clad with used directions and area 200×200 μm^2 which was observed using OIM can be seen in Figure 1. Lack of the fusion on the sides of the clad could be observed, it is probably the result of incorrect setting of laser power density.

Table 1: Chemical composition of the steel AISI H13 according ISO 4957 [4], the powder AISI H13 and the clad.

	Cr, Wt.%	Mo, Wt.%	Si, Wt.%	V, Wt.%	Mn, Wt.%	C, Wt.%
EN ISO 4957	4.80 – 5.50	1.20 – 1.50	0.80 – 1.20	0.85 – 1.15	0.25 – 0.50	0.35 – 0.42
Powder H13	5.10 ± 0.07	1.79 ± 0.08	0.92 ± 0.11	1.08 ± 0.02	0.45 ± 0.07	
Clad	3.77 ± 0.05	1.21 ± 0.05	0.72 ± 0.01	0.84 ± 0.03	0.62 ± 0.03	

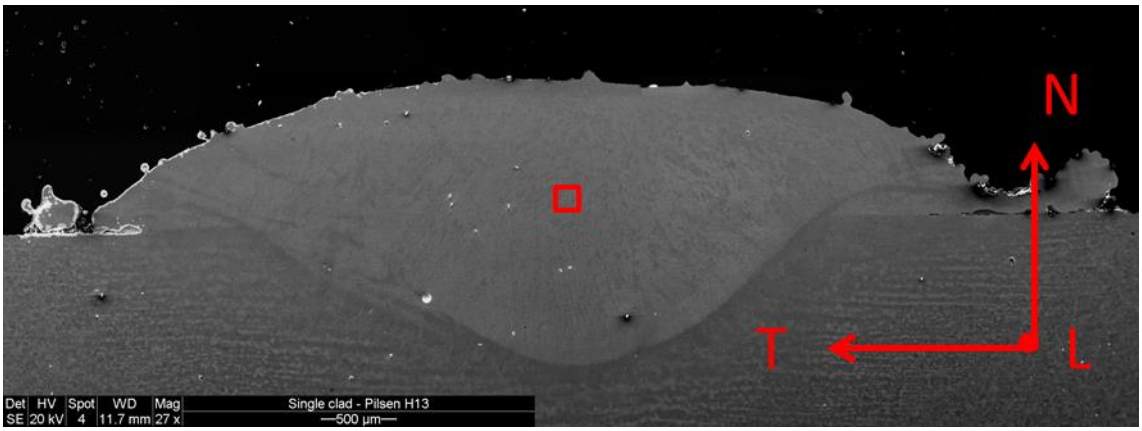

Fig. 1: SEM image of the cross-section of the single clad AISI H13 tool steel with marked directions and area which was observed using OIM.

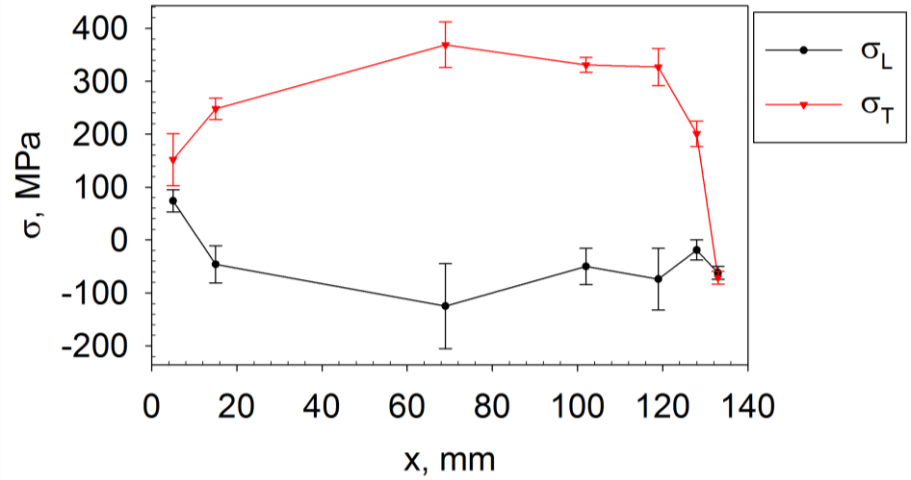

Fig. 2: Surface RS on the top of the clad in direction L and T, where *x* is the distance from the beginning of the clad.

The comparison of surface RS obtained by XRD in direction L and T is plotted in Figure 2. RS at the beginning and the end of the clad are almost equal within the error. In the direction L RS exhibit slight compressive stresses along the clad. However, in the direction T tensile RS were obtained. This dependence is opposite to what was generally observed in the literature [1, 5]. However, there were also published papers confirming tensile residual stresses in the perpendicular direction of the clads [6].

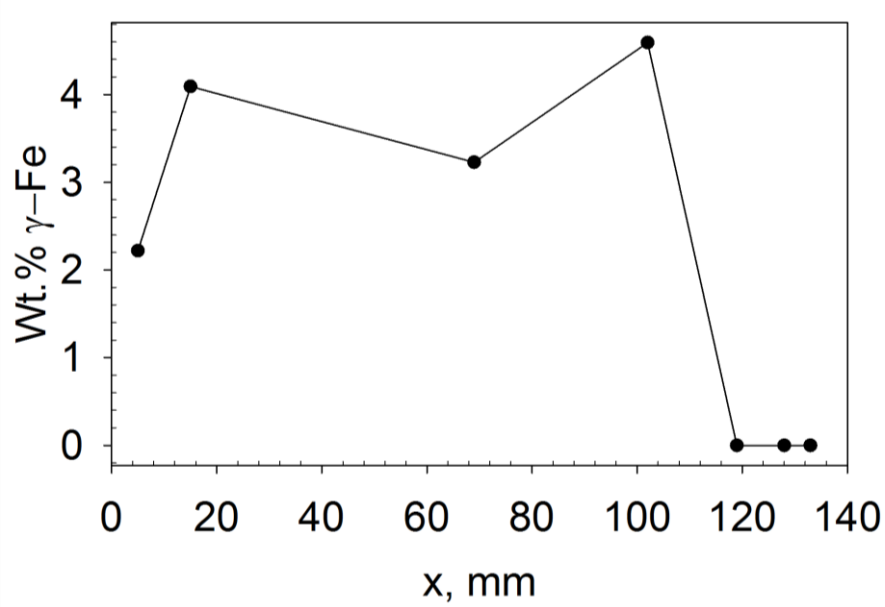

Fig. 3: Mass weight content of γ-Fe in the surface layer obtained by XRD.

Mass weight content of γ-Fe in the surface layer depending on the distance from the beginning of the clad is plotted in Figure 3. It may be observed that at the beginning of the clad a γ-Fe content is increasing to the value of around 4 %, and in the end no retained austenite was observed by XRD. This could be due to slower cooling rate at the end as the heating of the substrate occurred. After finding these results, the real structure and the microstructure of the single clad have been taken to deeper evaluation by OIM on the cross-section 5 mm from the beginning of the clad.

Figure 4 compares orientation maps of α-Fe in the selected area, wherein individual colours correspond to the normal vectors of planes that are parallel to the given direction. The original austenite grains, which were established during the transition of the melt into a solid phase and which subsequently disintegrated into martensitic laths are seen in the figure. Carbides of alloying elements were not observed using EBSD. However, in the analysed area, 1.1 % of retained austenite was confirmed. The difference compared to the value of XRD could be caused by an error of each method and by larger analysed volumes by XRD especially along the clad. At the beginning of the clad, proportion of retained austenite by XRD is growing.

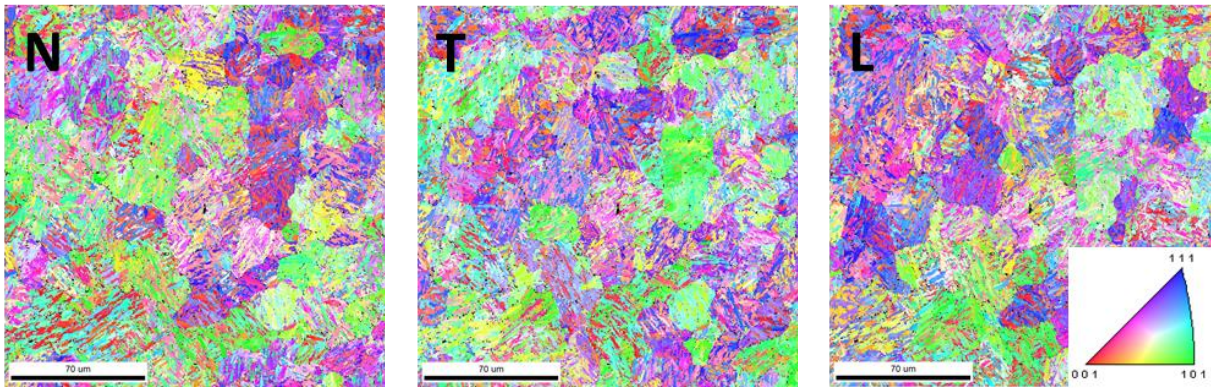

Fig. 4: Orientation maps of α-Fe for different directions in the selected area.

Figure 5 gives an idea of the relative representation of individual elements in the selected area obtained by energy-dispersive X-ray spectroscopy. Deeper colours indicate higher concentration of the element.

Subsequently, the distribution of the misorientation angle in the selected area is plotted in Figure 6. In the article [7], there was shown that misorientation angles between the variants that satisfy the Kurdjumov–Sachs orientation relationship of phase transformation between face-centered cubic and body-centered cubic are up to 21.06° and then higher than 47.11°.

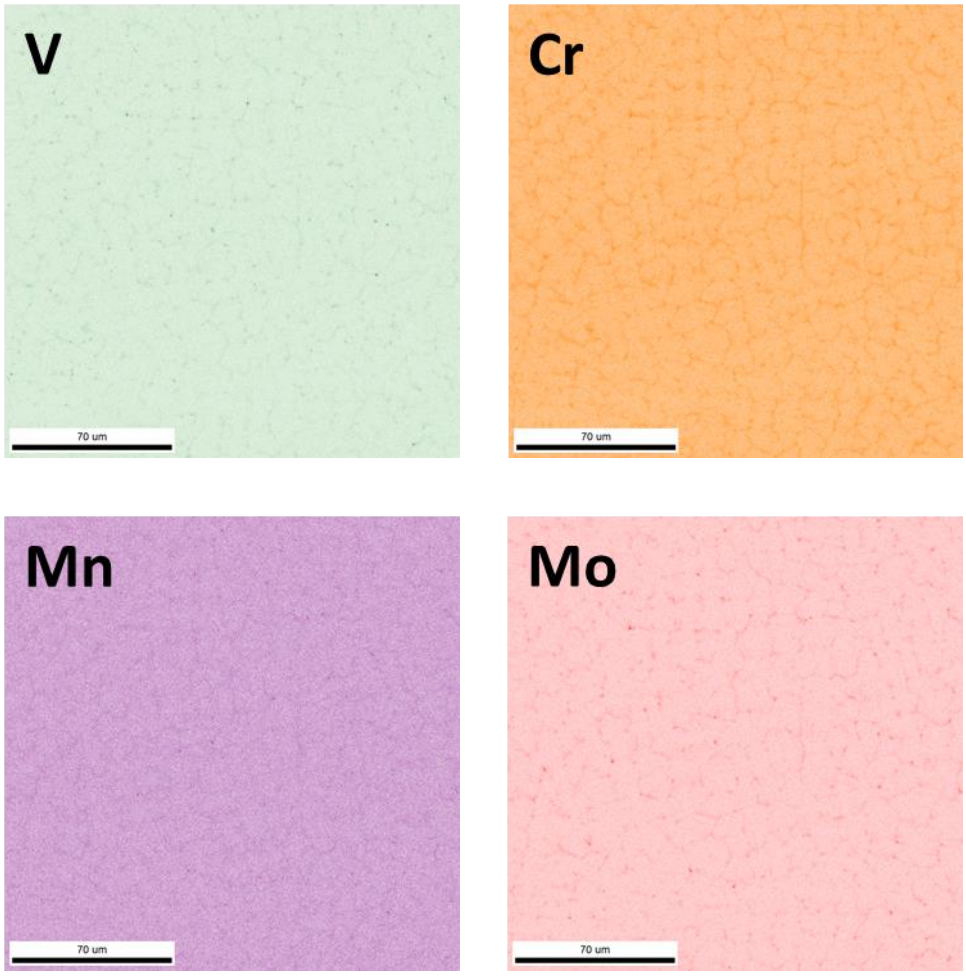

Fig. 5: Relative representation of content of selected elements in the selected area acquired by EDS.

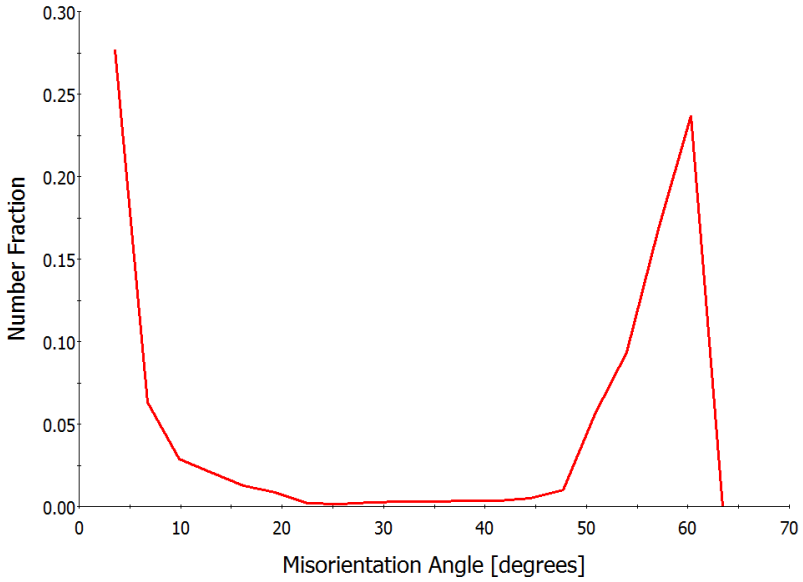

Fig. 6: Misorientation angle distribution in the selected area.

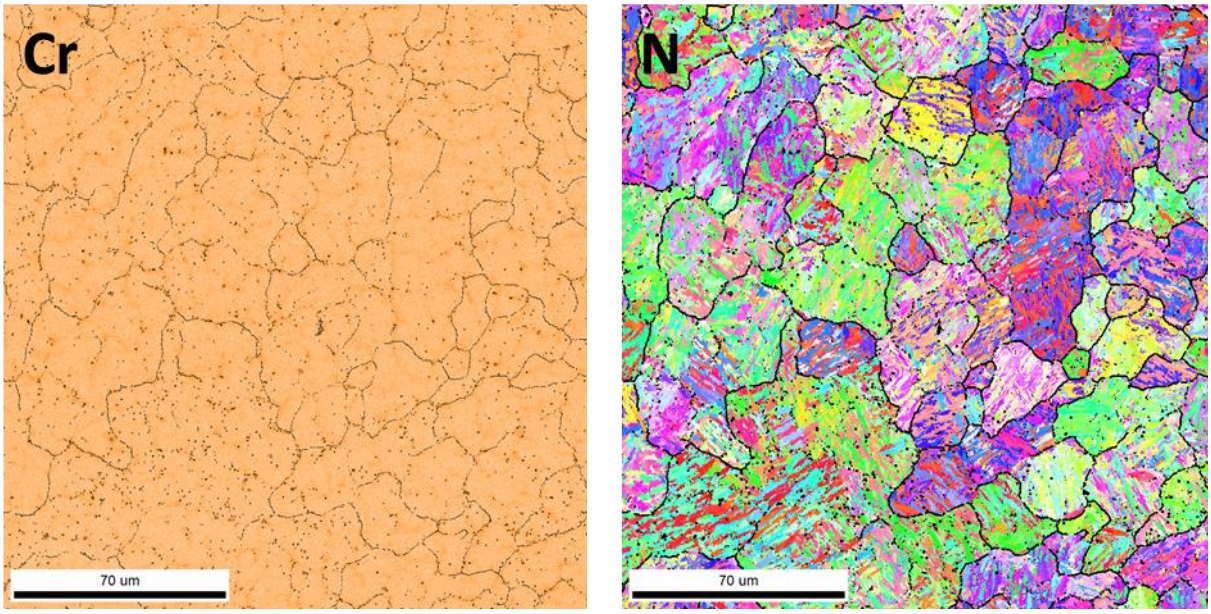

Fig. 7: Comparison of the map of relative representation of content of chromium and orientation map with highlighted grain boundaries between 21.2° and 47°.

Thus, Figure 7 compares a map of relative representation of content of chromium and orientation map with highlighted grain boundaries between 21.2° and 47°. It can therefore be clearly seen that higher concentration of chromium corresponds with the random grains boundaries between 21.2° and 47°. These boundaries correspond to the grain boundaries of the original austenitic grains which were formed during cooling of the melt. The unequal concentration of alloying elements is caused by the lever rule during solidification. This could induce inferior mechanical properties of the steel as carbides of alloying elements were not observed.

Previous results therefore suggest that there has been a rapid cooling of the melt to form a martensitic structure. Moreover, no carbides and half of the value of retained austenite in comparison with XRD were observed using EBSD. Therefore, it is concluded that in this case of laser cladding, phase transformation and not shrinkage is likely to be a dominant effect on

the formation of residual stress in the direction L along the clad. This caused the tensile RS in the perpendicular direction T.

Conclusions

Laser clad of the H13 tool steel showed great application potential. Martensitic structure was observed on the cross-section of the single clad. This suggests a high cooling rates and quenching of the clad. Laser cladding induced significant residual stresses. RS at the beginning and the end of the clad are almost equal within the error. In the direction L RS exhibit slight compressive stresses along the clad. However, in the direction T tensile RS were obtained. The research topic and the mainly the origin of residual stresses has not yet been accurately described and understood, so further measurements and adjusting the welding parameters will be needed.

Acknowledgement

Measurements were supported by the project TH02010664 of the Technology Agency of Czech Republic and by University of Groningen. This work was supported by the Student Grant Competition CTU in Prague grant No. SGS16/245/OHK4/3T/14.

References

[1] G. Telasang et al., Microstructure and mechanical properties of laser clad and post-cladding tempered AISI H13 tool steel, Metallurgical and Materials Transactions a-Physical Metallurgy and Materials Science 46A(5), pp. 2309-2321, 2015, DOI: 10.1007/s11661-015-2757-z.

[2] M. Vedani et al., Problems in laser repair-welding a surface-treated tool steel, Surface & Coatings Technology 201 (8), pp. 4518-4525, 2007, DOI: 10.1016/j.surfcoat.2006.09.051.

[3] Totten, G. E., Howes, M., Inoue, T., Handbook of residual stress and deformation of steel, Materials Park: ASM International, 2002, DOI: 10.1361/hrsd2002p027.

[4] ISO 4957:1999. Tool steels.

[5] J. Chen, S. Wang and L. Xue, On the development of microstructures and residual stresses during laser cladding and post-heat treatments, Journal of Materials Science 47(2), pp. 779-792, 2012, DOI: 10.1007/s10853-011-5854-4.

[6] A. Suárez et al., Study of residual stresses generated inside laser cladded plates using FEM and diffraction of synchrotron radiation, Surface & Coatings Technology 204(12), pp. 1983-1988, 2010, DOI: 10.1016/j.surfcoat.2009.11.037.

[7] H. Kitahara et al., Crystallographic features of lath martensite in low-carbon steel, Acta Materialia 54(5), pp. 1279-1288, 2006, DOI: 10.1016/j.actamat.2005.11.001.